

Engineering the Nanostructure of Molybdenum Nitride Nanodots Embedded N-Doped Porous Hollow Carbon Nanochains for Rapid All pH Hydrogen Evolution

Min-Qiang Wang¹, Chun Tang¹, Cui Ye², Jingjing Duan³, Changming Li¹, Yuming Chen⁴, Shu-Juan Bao^{1,3*}, and Maowen Xu^{1*}

¹ Institute for Clean Energy & Advanced Materials, Faculty of Materials and Energy, Southwest University
Chongqing 400715, PR China

*E-mail: xumaowen@swu.edu.cn; baoshj@swu.edu.cn

² Key Laboratory of Eco-Environments in Three Gorges Reservoir Region (Ministry of Education), School of Chemistry and Chemical Engineering, Southwest University
Chongqing 400715, PR China

³ Centre for Electrochemistry, Department of Chemistry
The University of Texas at Austin, Austin, TX 78712, USA

⁴ Department of Materials Science and Engineering
Massachusetts Institute of Technology
Cambridge, MA 02139, USA

Experimental section

Materials.

Analytical grade molybdenum oxide (MoO_3), molybdenyl acetylacetonate ($\text{C}_{10}\text{H}_{14}\text{MoO}_6$), N, N-Dimethylformamide (DMF), polyacrylonitrile (PAN) and tetraethyl orthosilicate were purchased from Aladdin Reagent (Shanghai, China). Ammonia, ethanol, and hydrofluoric acid (HF, 30%) were from Sinopharm Chemical Reagent Co., All chemicals were used without further purification. Double distilled water ($18.2 \text{ M}\Omega$) was used throughout the experiments.

Preparation of SiO_2 nanospheres

SiO_2 nanospheres were prepared by a modified Stöber method. Typically, 60 mL of deionized water, 20 mL of ethanol, and 12 mL of ammonia were mixed under stirring, then a mixture of 90 mL of ethanol and 6 mL of tetraethyl orthosilicate was added to this solution. After stirring for 4 h, SiO_2 nanospheres were washed by centrifugation (10,000 rpm, 10 min) with ethanol several times and dried under vacuum.

Preparation of MoN embedded N-doped porous carbon nanochains (MoN@NPCNCs), MoN embedded N-doped porous carbon nanofibers (MoN@NPCNFs), and bulk MoN.

To prepare MoN@NPCNCs, first, 1 mmol $\text{C}_{10}\text{H}_{14}\text{MoO}_6$ was dissolved in 5 mL DMF to form a green transparent solution by constant stirring, followed by the addition 250 mg SiO_2 nanospheres. Then, 350 mg PAN was added to the above solution. And the mixture were stirred at room temperature for 12 h to form a homogeneously solution. Then the precursor solution was subsequently electrospun at a constant flow rate of 0.4 mL h^{-1} and at a high voltage of 22 kV. The distance between the injector nozzle and the receiver was 16 cm, and the precursor of composite nanowires were collected on revolving aluminium foil. After drying at $100 \text{ }^\circ\text{C}$ for 12 h, the composite nanowires were presintered at $250 \text{ }^\circ\text{C}$ ($7 \text{ }^\circ\text{C min}^{-1}$) in air for 3 h. SiO_2 nanosphere was then etched by immersing the sample in 5 wt % HF solution for 6 h, and then the product was collected by vacuum filtration. The sample was then annealed for fully nitriding the MoN and carbonizing the decomposed PAN at $800 \text{ }^\circ\text{C}$ ($3 \text{ }^\circ\text{C min}^{-1}$) under an Ar/NH_3 flow (1:1 in volume ratio) atmosphere for 4 h.

MoN@NPCNFs was obtained with the same method of MoN@NPCNCs without the addition of SiO₂ nanospheres. Bulk MoN was prepared by annealing the commercial MoO₃ at 800 °C (3 °C min⁻¹) under an Ar/NH₃ flow (1:1 in volume ratio) atmosphere for 4 h.

Material characterization

The electrospinning device consists of a high voltage power supply (DW-P503-1ACCC, Dongwen, Tianjin, China) and a syringe pump (model 11 Plus, Harvard apparatus U.S.A.). The crystal structures of the products were determined by powder X-ray diffraction (XRD, Shimadzu XRD-7000, Japan). The structures and morphologies of prepared nanohybrids were sequentially assessed using field-emission scanning electron microscopy (FESEM, JEOL-7800F, Japan Electron Optics Laboratory Co., Japan), energy-dispersive X-ray spectroscopy (EDX, INCA X-Max 250, Japan), and transmission electron microscope (TEM, JEM-2100, Japan). The Brunauer–Emmett–Teller (BET) surface area was measured by using Quadrasorb evo 2QDS-MP-30 (Quantachrome Instruments, USA). Pore-size-distribution (PSD) plots were obtained from the adsorption branch of the isotherm using the Barrett–Joyner–Halenda (BJH) model. The surface properties of the samples were studied by X-ray photoelectron spectroscopy (XPS, Escalab 250xi, Thermo Scientific). Thermogravimetric analysis was performed on Thermo Gravimetric Analyzer (TGA, Q50, USA) at a rate of 5 °C min⁻¹ under air from 30 to 650 °C.

Electrochemical Performance

The glassy carbon (GC, $\Phi = 5.6$ mm) electrode was respectively polished with 0.3 and 0.05mm alumina slurry followed by rinsing thoroughly with double distilled water, and then ultrasonically cleaned in ethanol and double distilled water to obtain a mirrorlike surface. The as-prepared bulk MoN, MoN@NPCNFs, MoN@NPCNCs and commercial Pt/C ethanol dispersion (15 μ L, 5mg mL⁻¹) that containing 1 wt % Nafion was dropped onto the well-polished bare GCE, respectively, and then evaporated in air as working electrode. The electrochemical tests were executed by a workstation (CHI660E, CHI Instruments Inc, Shanghai) in a three-electrode setup coupled with bulk MoN-GC, MoN@NPCNFs-GC, and MoN@NPCNCs-GC as a working electrode,

respectively. Graphite electrode as a counter electrode and saturated calomel electrode (SCE) as a reference electrode. The polarization curves were surveyed *via* the linear sweep voltammetry (LSV) at a scan rate of 2 mV s⁻¹, and the long-term durability was investigated using potentiostatic electrolysis at fixed potentials. The current density was calibrated corresponding to the geometric area of working electrode. The geometric area values of all the samples are all 0.2462 cm². The value of current density is calculated *via* dividing the current by geometric area. The recorded potential was adjusted by this equation: $E(\text{RHE}) = E(\text{SCE}) + (0.242 + 0.059 \text{ pH}) \text{ V}$. The Tafel slopes, derived from a linear fit utilizing the Tafel equation ($\eta = b \log j + a$, where η is the overpotential, b is the Tafel slope, and j is the current density). Electrochemical impedance spectroscopy (EIS) measurements were carried out from 1000 kHz to 0.1 Hz with an amplitude of 10 mV at the open-circuit voltage in a 0.5 M H₂SO₄ solution. The electrochemical double-layer capacitances (C_{dl}) of catalysts were calculated from CV curves. The CV curves were performed at scan rates varying from 10 to 100 mV s⁻¹ in the region from 0.07 to 0.27 V vs RHE.

Hydrogen production measurement.

The amount of hydrogen produced during electrochemical water splitting was measured via an online gas chromatograph (GC-2014, Shimadzu). The cell setup was the same as that used for electrochemical measurements.

Computational Methods:

Spin-polarized density functional theory calculations were performed using the Vienna ab initio simulation package (VASP)¹⁻³. We used the PBE functional for the exchange–correlation energy⁴ and projector augmented wave (PAW) potentials^{5,6}. The kinetic energy cutoff was set to 500 eV. The ionic relaxation was performed until the force on each atom is less than 0.01 eV Å⁻¹. The k-point meshes were 3 × 3 × 1 with the Monkhorst–Pack method⁷. To minimize the undesired interactions between images, a vacuum of at least 15 Å was considered along the z axis. Our calculations indicate that the surface energies (E_{surf}) of the (001), (011), (100), (1010), (110), and (111) facets are 208.0, 157.8, 195.4, 140.2, 168.3, and 166.5 meV Å⁻², respectively.

$$E_{surf} = (E_{slab} - N E_{bulk}) / 2S,$$

in which S is the surface area, E_{slab} is the energy of bulk MoN, and E_{bulk} is the energy of the model used in our calculations. In our model, we chose the (101) facet to interpret the reaction mechanism, mainly because the E_{surf} of the (101) surface is relatively lower, indicating that it is thermodynamically the most stable.

The free energy change for H^* adsorption on both surfaces (ΔG_H) was calculated as follows, which is proposed by Norskov and coworkers⁸:

$$\Delta G_H = E_{total} - E_{sur} - E_{H_2}/2 + \Delta E_{ZPE} - T\Delta S$$

where E_{total} is the total energy for the adsorption state, E_{sur} is the energy of the corresponding surface, E_{H_2} is the energy of H_2 in gas phase, ΔE_{ZPE} is the zero-point energy change and ΔS is the entropy change.

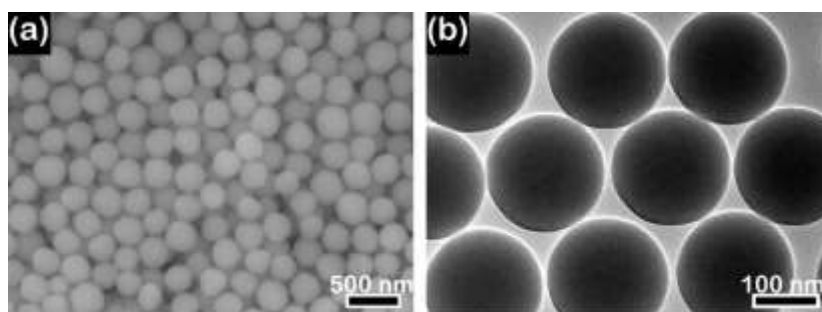


Figure S1. FESEM (a) image and TEM (b) image of as-prepared SiO₂ nanospheres

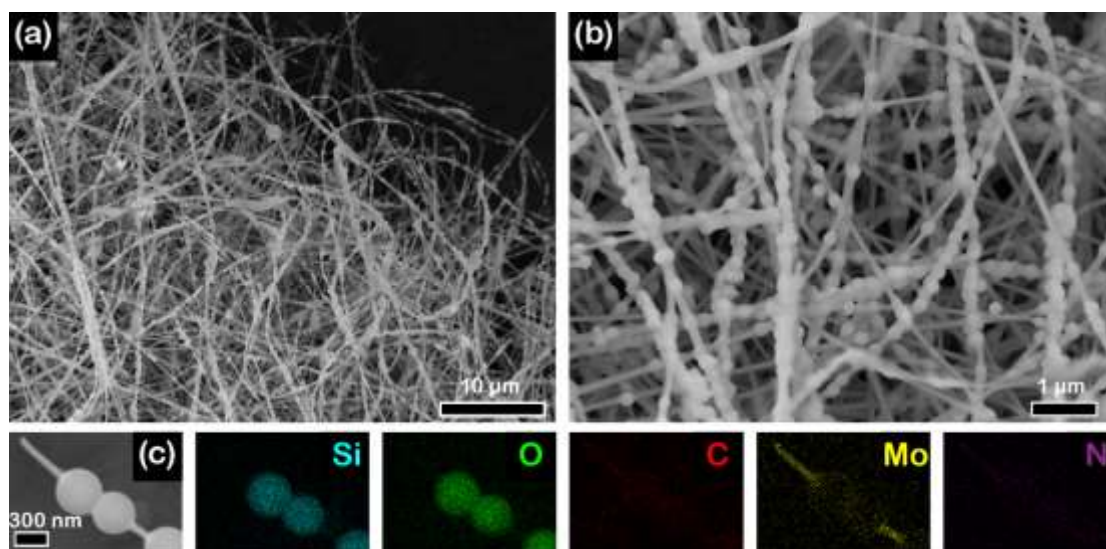


Figure S2. Low-resolution (a), high-resolution (b) FESEM, and EDS element mapping (c) images of as-prepared Mo-SiO₂-PAN

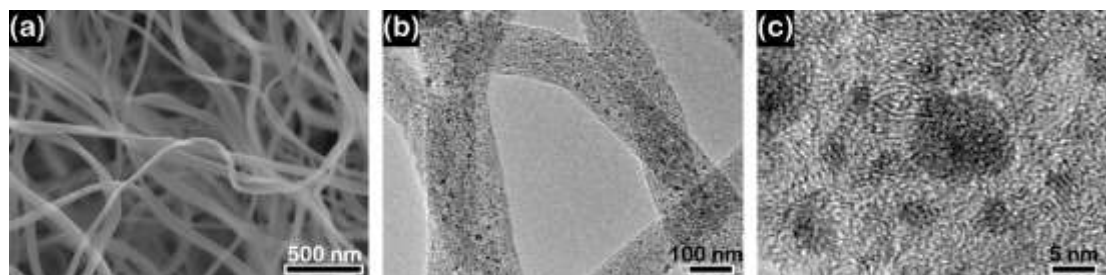


Figure S3. FESEM (a), low-resolution (b), and high-resolution (c) TEM images of MoN@NPCNFs.

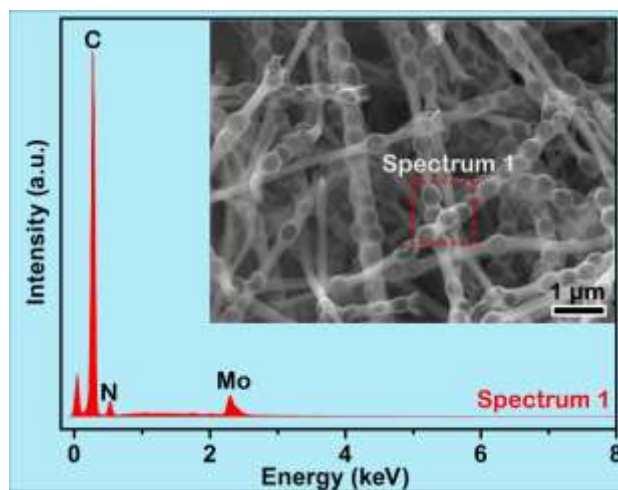


Figure S4. EDS spectrum of MoN@NPCNCs. Inset is the FESEM image of MoN@NPCNCs, red frame represents the EDS spectrum area.

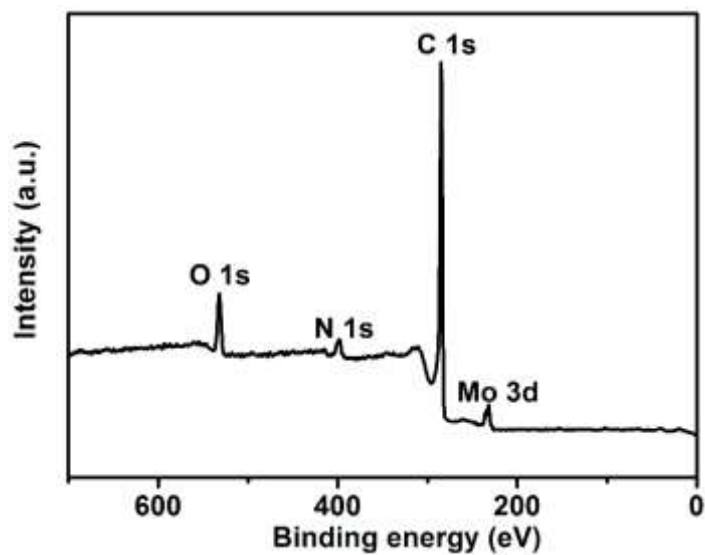


Figure S5. XPS survey scan of MoN@NPCNCs

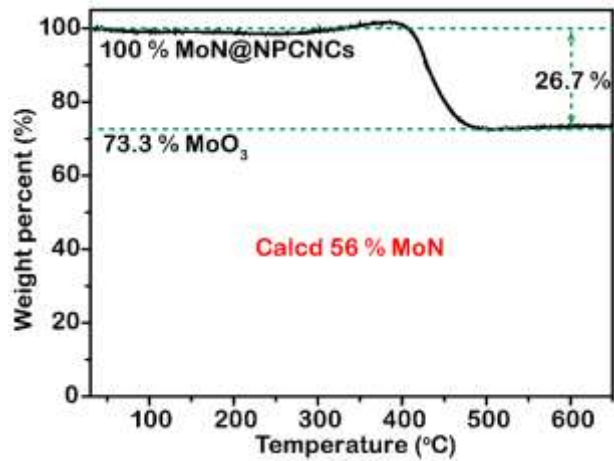


Figure S6. TGA curve of MoN@NPCNCs in air atmosphere

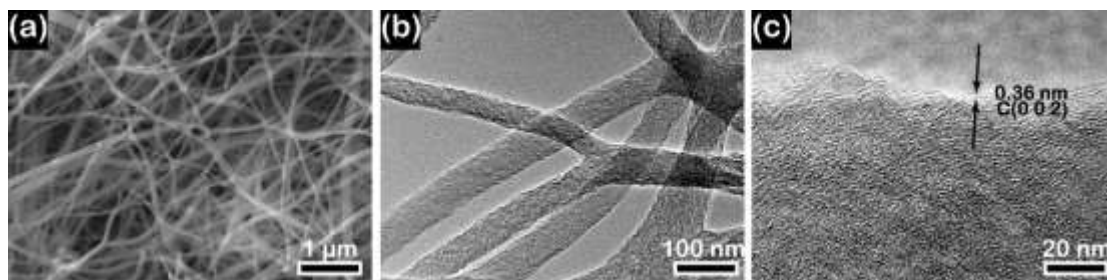


Figure S7. FESEM (a), low-resolution (b), and high-resolution (c) TEM images of NCNFs.

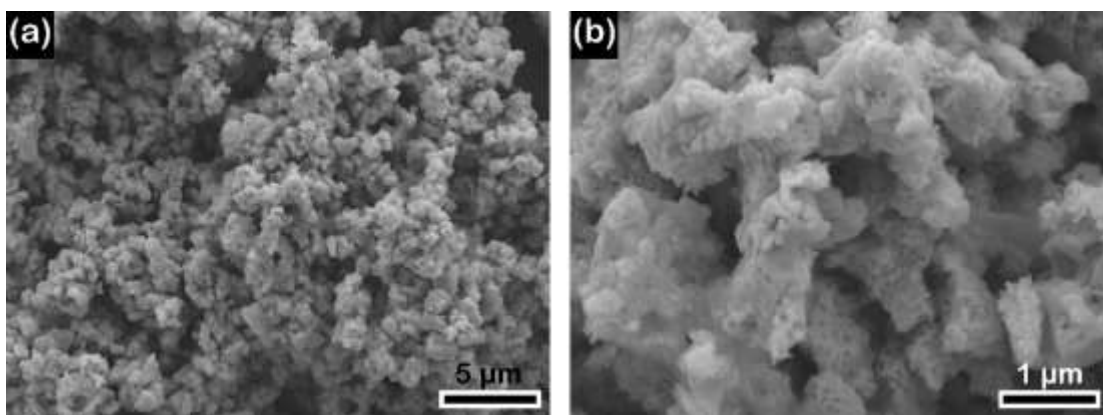


Figure S8. Low-resolution (a), high-resolution (b) FESEM, images of as-prepared bulk MoN.

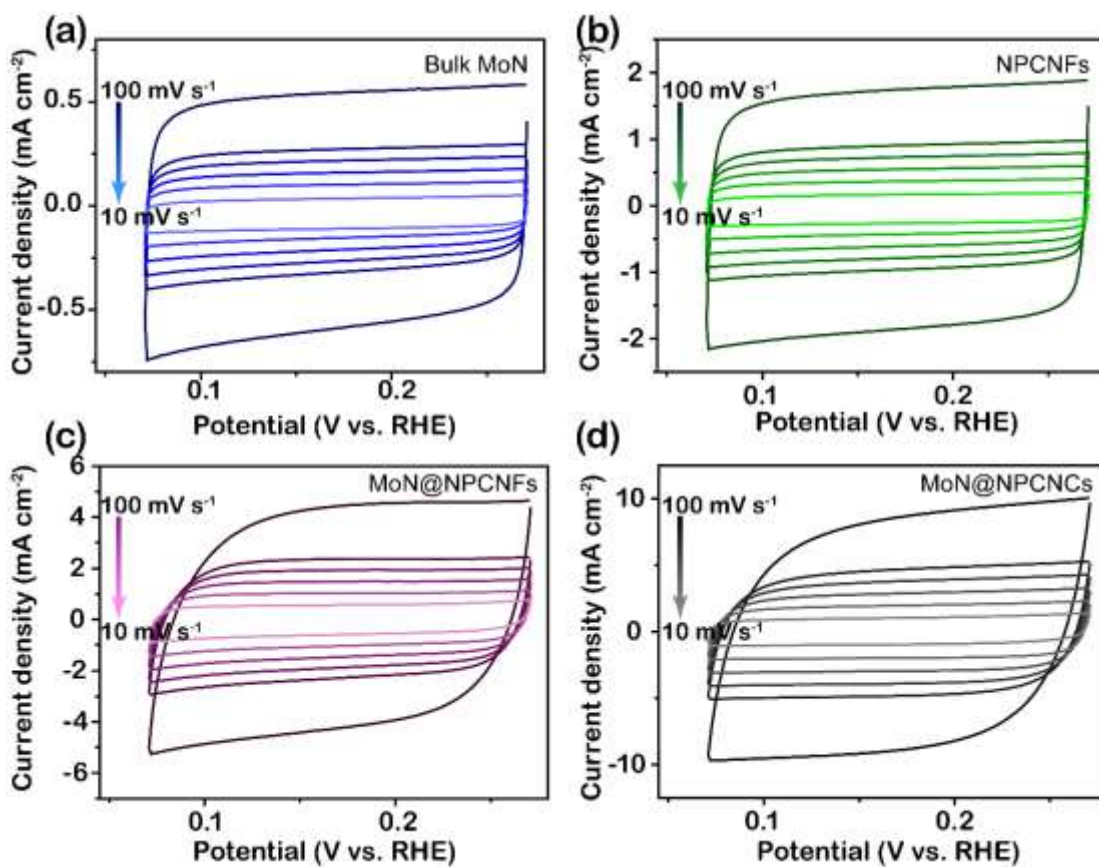


Figure S9. Cyclic voltammograms for (a) bulk MoN, (b) NPCNFs, (c) MoN@NPCNFs, and (d) MoN@NPCNCs in the non-Faradaic capacitance current range at scan rates from 10 to 100 mV s^{-1} .

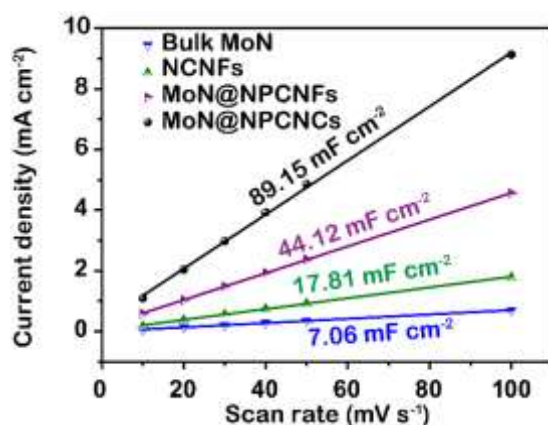


Figure S10. Capacitive currents as a function of scan rate for NCNFs, bulk MoN, MoN@NPCNFs, and MoN@NPCNCs.

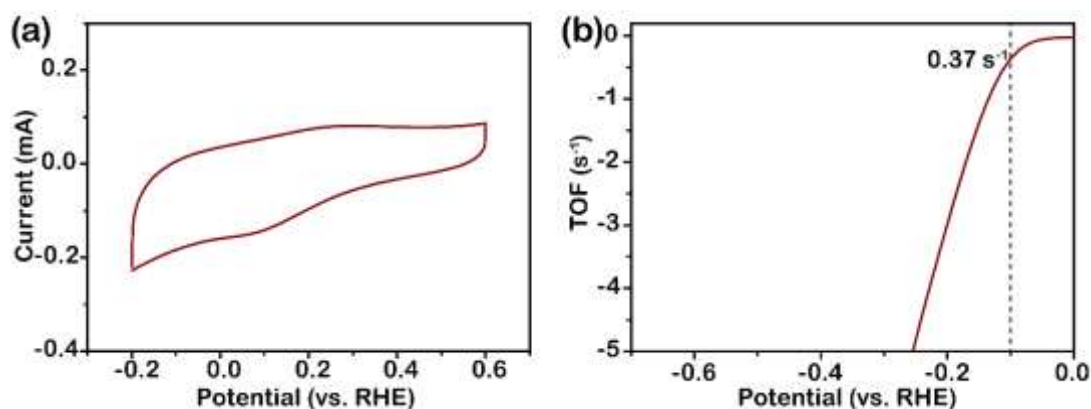


Figure S11. (a) Cyclic voltammograms of MoN@NPCNCs in 1 M PBS (pH = 7) with a scan rate of 50 mV s^{-1} . (b) Calculated TOF for MoN@NPCNCs in $0.5 \text{ M H}_2\text{SO}_4$.

The intrinsic catalytic activity is measured by the turnover frequency (TOF) for each active site. We attempted to quantify the active sites by electrochemistry. Figure S11a shows the cyclic voltammograms in the region of -0.2 V to 0.6 V vs. RHE for the MoN@NPCNCs at pH = 7. The integrated charge over the whole potential range should be proportional to the total number of active sites. Assuming a one electron process for both reduction and oxidation, the upper limit of active sites could be calculated. Figure S11b shows the polarization curves at pH = 0 normalized by the active sites, and expressed in terms of TOF. The values of TOF at 100 mV are 0.37 s^{-1} in acidic media,

which are better than those of Mo-based catalysts, such as Mo₂N–Mo₂C heterojunction, [Mo₃S₁₃]²⁻, and MoP/S⁹⁻¹¹

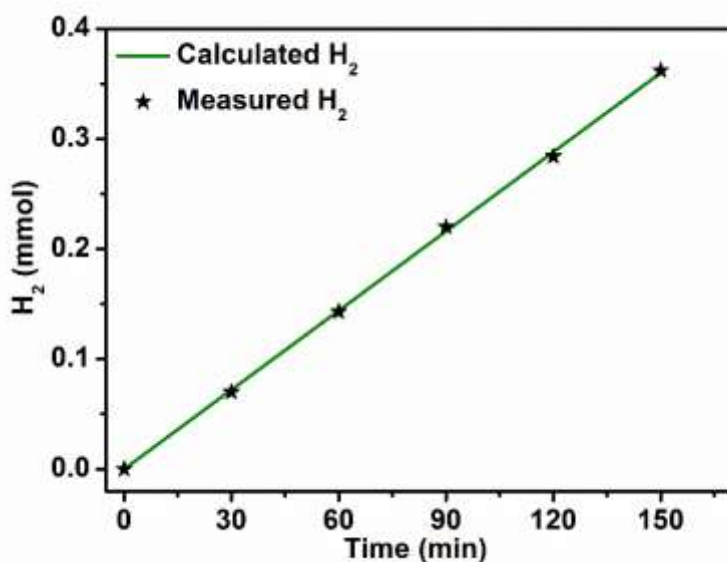


Figure S12 The amount of theoretically calculated (green curve) and experimentally measured (black stars) hydrogen versus time for MoN@NPCNCs at -0.3 V in 0.5 M H₂SO₄.

The amount of hydrogen produced through electrochemical water splitting was measured quantitatively using gas chromatography (GC). The Faradaic efficiency (FE) of the HER process can be obtained by dividing the measured amount of hydrogen with calculated one (assuming 100 % FE). The excellent agreement of the two sets of values (Figure S*) indicates that the FE is close to 100 %.

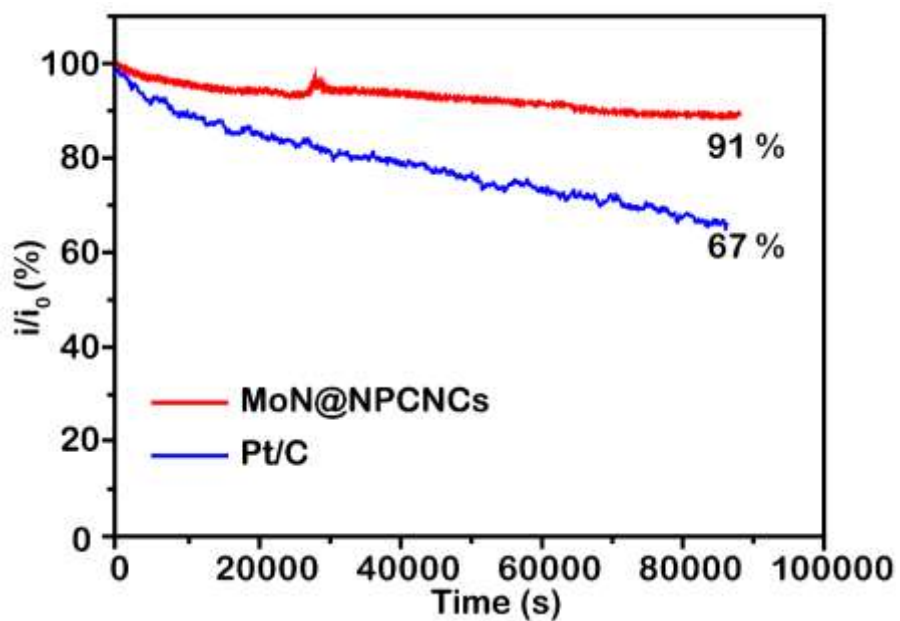


Figure S13. Current density-time (I-t) curve of MoN@NPCNCs and Pt/C in 0.5 M H₂SO₄

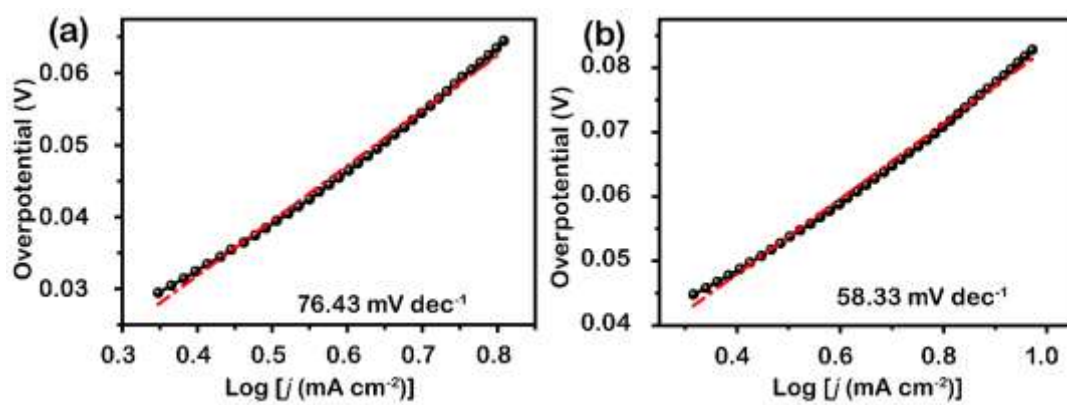


Figure S14 Tafel plots for MoN@NPCNCs in (a) PBS (pH=7, 1.0 M) and (b) KOH (pH=14, 1.0 M), respectively.

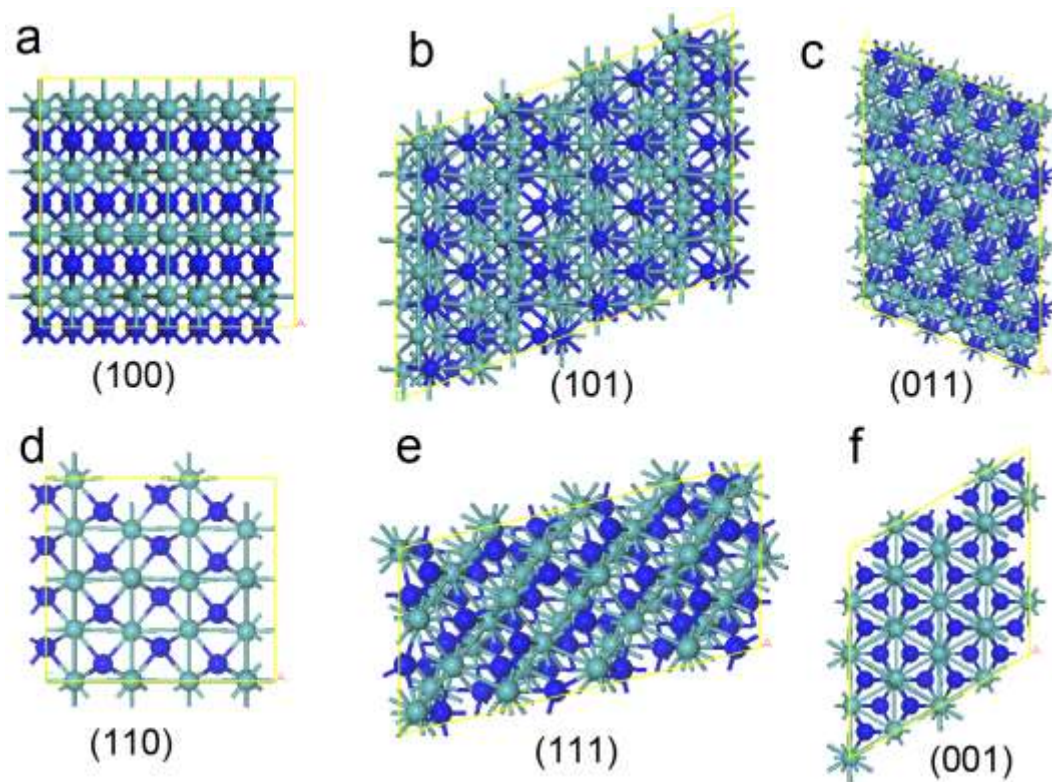


Figure S15. Top views of clean MoN surfaces. Mo, cyan; N, blue.

Table S1 Comparison of HER performance in acidic media for MoN@NPCNCs with other HER electrocatalysts

Catalyst	Tafel slope (mV dec ⁻¹)	Current density (<i>j</i> , mA cm ⁻²)	η at the corresponding <i>j</i> (mV)	Ref.
CoP hollow polyhedron	59	1	70	12
		10	159	
NiSe ₂ /Ni hybrid foams	49	10	143	13
Mo ₂ C@C	56	10	141	14
MoC-Mo ₂ C-31.4	43	10	126	15
Ni-P nanoparticles	102	2	57	16
		10	362	
NiCo ₂ P _x Nanowires	57.7	10	104	17
graphene-Mo ₂ C rods	67	10	206	18
Co ₉ S ₈ @MoS ₂	110	10	190	19
se-MoS ₂	59	10	104	20
MoS ₂ grown on graphene	41	10	100	21
MoS _{0.86} P _{0.57} /CB	57	10	120	22
		20	135	
MoS ₂	62	10	170	23
Mo ₂ C/C	82	10	180	24
Fe/P/C _{0.5-800}	35.9	1	131	25
		10	256	
Ni _{0.3} Mo _{0.7} O ₃	114	40	400	26
FeP nanosheets	67	10	240	27
MoN@NPCNCs	53.21	10	72	This work

Table S2 Comparison of HER performance in neutral media for MoN@NPCNCs with other HER electrocatalysts

Catalyst	Tafel slope (mV dec ⁻¹)	Current density (<i>j</i> , mA cm ⁻²)	η at the corresponding <i>j</i> (mV)	Ref.
CoN _x /C	247	10	75	28
FeP NAs NW/CC	202	10	71	29
CoP/Ti	149	10	58	30
Co-C-N complex	273	10	107	31
MoS _{2.7} @NPG	350	10	60	32
MoN@NPCNCs	76.43	10	84.85	This work

Table S3 Comparison of HER performance in alkaline media for MoN@NPCNCs with other HER electrocatalysts

Catalyst	Tafel slope (mV dec ⁻¹)	Current density (<i>j</i> , mA cm ⁻²)	η at the corresponding <i>j</i> (mV)	Ref.
NiFeOx/CFP	118	10	88	33
Co-P film	120	10	94	34
Ni/NiS	115	10	230	35
CoOx@CN	82	10	232	36
CP@Ni-P	60	10	117	37
MoN@NPCNCs	58.33	10	80.18	This work

References

1. G. Kresse and J. Furthmüller, *Comp.mat.er.sci*, 1996, **6**, 15-50.
2. G. Kresse and J. Furthmüller, *Phys Rev B Condens Matter*, 1996, **54**, 11169-11186.
3. G. Kresse and J. Hafner, *Physical Review B Condensed Matter*, 1994, **49**, 14251.
4. J. P. Perdew, K. Burke and M. Ernzerhof, *Physical Review Letters*, 1998, **77**, 3865-3868.
5. G. Kresse, *Phys.rev.b*, 1999, **59**, 1758-1775.
6. B. PE, *Phys Rev B Condens Matter*, 1994, **50**, 17953-17979.
7. H. J. Monkhorst, *Physical Review B Condensed Matter*, 1976, **16**, 1748-1749.
8. n.-A. M. Cabã, M. L. Stone, J. R. Schmidt, J. G. Thomas, Q. Ding, H. C. Chang, M. L. Tsai, J. H. He and S. Jin, *Nature Materials*, 2015, **14**, 1245-1251.
9. H. Yan, Y. Xie, Y. Jiao, A. Wu, C. Tian, X. Zhang, L. Wang and H. Fu, *Advanced Materials*, 2018, **30**, 1704156.
10. J. Kibsgaard, T. F. Jaramillo and F. Besenbacher, *Nature chemistry*, 2014, **6**, 248-253.
11. J. Kibsgaard and T. F. Jaramillo, *Angew Chem Int Ed Engl*, 2014, **53**, 14433-14437.
12. M. Liu and J. Li, *Acs Applied Materials & Interfaces*, 2016, **8**, 2158-2165.
13. H. Zhou, Y. Wang, R. He, F. Yu, J. Sun, F. Wang, Y. Lan, Z. Ren and S. Chen, *Nano Energy*, 2016, **20**, 29-36.
14. Y. Y. Chen, Y. Zhang, W. J. Jiang, X. Zhang, Z. Dai, L. J. Wan and J. S. Hu, *Acs Nano*, 2016, **10**, 8851.
15. H. Lin, Z. Shi, S. He, X. Yu, S. Wang, Q. Gao and Y. Tang, *Chemical Science*, 2016, **7**, 3399-3405.
16. L. Wan, J. Zhang, Y. Chen, C. Zhong, W. Hu and Y. Deng, *Journal of Materials Science*, 2016, **52**, 1-11.
17. R. Zhang, X. Wang, S. Yu, T. Wen, X. Zhu, F. Yang, X. Sun, X. Wang and W. Hu, *Advanced Materials*, 2016, **29**, 1605502.
18. K. Ojha, S. Saha, H. Kolev, B. Kumar and A. K. Ganguli, *Electrochimica Acta*,

- 2016, **193**, 268-274.
19. H. Zhu, J. Zhang, R. Yanzhang, M. Du, Q. Wang, G. Gao, J. Wu, G. Wu, M. Zhang and B. Liu, *Advanced Materials*, 2015, **27**, 4752.
 20. J. Hu, B. Huang, C. Zhang, Z. Wang, Y. An, D. Zhou, H. Lin, M. K. H. Leung and S. Yang, *Energy & Environmental Science*, 2017, **10**.
 21. A. Behranginia, M. Asadi, C. Liu, P. Yasaei, B. Kumar, P. Phillips, T. Foroozan, J. C. Waranius, K. Kim and J. Abiade, *Chemistry of Materials*, 2016, **28**.
 22. R. Ye, A. P. Del, Y. Liu, M. J. Arellanojimenez, Z. Peng, T. Wang, Y. Li, B. I. Yakobson, S. H. Wei and M. J. Yacaman, *Advanced Materials*, 2016, **28**, 1427-1432.
 23. D. Kiriya, P. Lobaccaro, H. Y. Nyein, P. Taheri, M. Hettick, H. Shiraki, C. M. Sutter-Fella, P. Zhao, W. Gao and R. Maboudian, *Nano Letters*, 2016, **16**, 4047.
 24. S. Tuomi, R. Guil-Lopez and T. Kallio, *Journal of Catalysis*, 2016, **334**, 102-109.
 25. M. Li, T. Liu, X. Bo, M. Zhou, L. Guo and S. Guo, *Nano Energy*, 2017, **33**, 221-228.
 26. A. K. Kunhiraman and M. Ramasamy, *Journal of Nanoparticle Research*, 2017, **19**, 203.
 27. Y. Xu, R. Wu, J. Zhang, Y. Shi and B. Zhang, *Chemical Communications*, 2013, **49**, 6656-6658.
 28. H. W. Liang, S. Brüller, R. Dong, J. Zhang, X. Feng and K. Müllen, *Nature Communications*, 2015, **6**, 7992.
 29. Y. Liang, Q. Liu, A. M. Asiri, X. Sun and Y. Luo, *Acs Catalysis*, 2014, **4**, 4065-4069.
 30. Z. Pu, Q. Liu, P. Jiang, A. M. Asiri, A. Y. Obaid and X. Sun, *Chemistry of Materials*, 2014, **26**, 4326-4329.
 31. Z. Wang, X. F. Hao, Z. Jiang, X. P. Sun, D. Xu, J. Wang, H. Zhong, F. L. Meng and X. Zhang, *Journal of the American Chemical Society*, 2015, **137**, 15070-15073.
 32. X. Ge, L. Chen, L. Zhang, Y. Wen, A. Hirata and M. Chen, *Advanced Materials*,

- 2014, **26**, 3100-3104.
33. H. Wang, H. W. Lee, Y. Deng, Z. Lu, P. C. Hsu, Y. Liu, D. Lin and Y. Cui, *Nature Communications*, 2015, **6**, 7261.
 34. N. Jiang, B. You, M. Sheng and Y. Sun, *Angewandte Chemie*, 2015, **54**, 6251-6254.
 35. G. F. Chen, T. Y. Ma, Z. Q. Liu, N. Li, Y. Z. Su, K. Davey and S. Z. Qiao, *Advanced Functional Materials*, 2016, **26**, 3314-3323.
 36. H. Jin, J. Wang, D. Su, Z. Wei, Z. Pang and Y. Wang, *Journal of the American Chemical Society*, 2015, **137**, 2688-2694.
 37. X. Wang, W. Li, D. Xiong, D. Y. Petrovykh and L. Liu, *Advanced Functional Materials*, 2016, **26**, 4067-4077.